Theory of bound magnetic polarons in cubic and uniaxial antiferromagnets

Dawid Bugajewski, $^{1,\,*}$ Carmine Autieri, $^{2,\,\dagger}$ and Tomasz Dietl $^{2,\,\ddagger}$

¹Faculty of Physics, University of Warsaw, Pasteura 5, PL-02093 Warsaw, Poland ²International Research Centre MagTop, Institute of Physics, Polish Academy of Sciences, Aleja Lotnikow 32/46, PL-02668 Warsaw, Poland (Dated: October 28, 2025)

Motivated by a recent debate about the origin of remanent magnetization and the corresponding anomalous Hall effect in antiferromagnets and altermagnets, a theory of bound magnetic polarons (BMPs) in anisotropic magnetic semiconductors is developed. The theory describes quantitatively the experimentally observed magnitude of excess magnetization and its dependence on the magnetic field in cubic antiferromagnetic EuTe. In contrast to the cubic case, our theory predicts the presence of magnetization hysteresis below Néel temperature in antiferromagnets with uniaxial anisotropy. We show, employing material parameters implied by experimental and *ab initio* results, that the magnitudes of remanent magnetization and the coercive field are in accord with recent experimental observations for altermagnetic hexagonal MnTe. While the altermagnets have an intrinsic contribution to the remanent magnetization and the anomalous Hall effect, our theory explains the origin of an extrinsic contribution. Our findings address, therefore, a question about the relative contribution to the remanent magnetization of bound magnetic polarons and weak ferromagnetism driven by the antisymmetric exchange interaction, the latter weakened by the formation of antiferromagnetic domains. Furthermore, we provide the theory of BMP spontaneous spin splitting, which can be probed optically.

Owing to strong sensitivity to doping, gating, and illumination on the one hand, and the presence of exchange split bands and generally high spin-ordering temperatures on the other, altermagnetic semiconductors [1, 2] constitute an appealing alternative to ferromagnetic semiconductors [3, 4] in search for new spintronic functionalities and relevant materials systems. A lot of recent attention has been devoted to new aspects of free magnetic polarons in antiferromagnets [5–10] and altermagnets [11], earlier studied in the context of copper oxide superconductors [12]. However, one of the pertinent questions concerns the possibility of controlling magnetic properties by changing the occupation of in-gap impurity of defect states.

In this Letter, we develop the theory of bound magnetic polarons (BMPs) for the case of antiferromagnetic and altermagnetic semiconductors containing singly-occupied impurity states, extending previous approaches [13-18] in two ways. First, we consider an experimentally relevant low-crystal symmetry case, such as hexagonal MnTe, in which, as we find, the presence of BMPs can lead to hysteretic ferromagnetic-like properties. Second, by taking into account thermodynamic fluctuations of magnetization, we go beyond both the zerotemperature limit and the mean-field approximation, an essential step at non-zero temperatures due to the finite size of BMP. Furthermore, we are interested in the thermal equilibrium case, so that the excitonic BMP, examined in a series of experimental and theoretical works in the context of EuTe luminescence [19], is not discussed here. Our starting point is the previous theory of BMPs in a paramagnetic phase [20–22], which has successfully described spin dynamics of quantum-dot electrons immersed in a bath of nuclear spins [23] and earlier optical, charge transport, and magnetic properties observed in dilute magnetic semiconductors [24]. Interestingly, the BMP case constitutes an experimental realization of the central spin problem [25], a persistent challenge of quantum statistical physics [26]. However, it is worth noting in this context that the semiclassical approach, within which the central spin s is treated quantum mechanically whereas the surrounding spins S classically, is quantitatively accurate for a dozen or more spins S even if S=1/2 provided that the statistical sum is calculated exactly, i.e., without, for instance, a mean-field approximation [23].

We show that the theory describes the time-honored observations of excess magnetization and its dependence on the magnetic field in cubic antiferromagnetic EuTe below Néel temperature T_N [27, 28]. In order to apply our results to altermagnetic hexagonal MnTe, we determine exchange integrals J accounting for spin splittings of bands from first-principle computations. Making use of J values and taking other relevant parameters from experimental data [29–31], we show that our theory describes properly the experimentally found [32] orientation and magnitude of remanent magnetization M_r along the hexagonal c axis and the observed value of the coercive field H_c , also available from Hall resistance studies [32, 33]. We conclude that spin and orbital magnetization expected in MnTe from the antisymmetric exchange interactions [34, 35] either compete with the BMP contribution or are masked by the formation of domains with antiparallel in-plane Néel vectors, which results in a cancellation of magnetization resulting from spin canting

 $^{^{*}}$ d.bugajewski@student.uw.edu.pl

 $^{^{\}dagger}$ autieri@MagTop.ifpan.edu.pl

[‡] dietl@MagTop.ifpan.edu.pl

along the c axis driven by the antisymmetric exchange interactions. Such a cancellation does not occur in the case of BMPs, as the orientation of BMPs' magnetization along the c-axis is independent of the in-plane Néel vector direction.

Theory of bound magnetic polarons in antiferromagnetic semiconductors. We assume that in the case of antiferromagnets and altermagnets there are no spontaneous spin splittings at the band extrema, so that, a non-zero value of magnetization is necessary to generate spin splitting of a carrier bound to an impurity or defect. We adopt, therefore, the magnetization of localized spins $\vec{M}(\vec{r})$ as an order parameter. For an effective-mass carrier bound to a singly ionized impurity, the BMP free energy assumes the form $F_{\rm BMP} = E_{\rm imp} + F_p$, where

$$E_{\rm imp} = \langle \Psi | \frac{\hat{p}^2}{2m^*} - \frac{e^2}{\epsilon r} | \Psi \rangle, \tag{1}$$

whereas F_p is given by a functional integral over magnetization profiles [21],

$$F_p = -k_{\rm B}T \ln \int \mathcal{D}\vec{M}(\vec{r}) P_p[\vec{M}(\vec{r})] / P_S[\vec{M}(\vec{r})].$$
 (2)

The probability distribution P_S of the localized spins' magnetization is determined by the free energy functional $\mathcal{F}_S[\vec{M}(\vec{r})]$, whose form can be determined from the experimental dependence of magnetization on the magnetic field in the absence of BMPs [36]. The distribution P_p takes into account the presence of a bound carrier with a spin s = 1/2, according to

$$P_p[\vec{M}(\vec{r})] = \exp(-\mathcal{F}_S[\vec{M}(\vec{r})]/k_{\rm B}T)2\cosh(\Delta[\vec{M}(\vec{r})]/2k_{\rm B}T), (3)$$

where the bound carrier spin splitting $\bar{\Delta}$ is given by,

$$\vec{\Delta}[\vec{M}(\vec{r})] = \frac{1}{g\mu_B} \int d\vec{r} J \vec{M}(\vec{r}) |\Psi(\vec{r})|^2 d\vec{r} + g^* \mu_B \vec{H}. \quad (4)$$

Here, g, g^*, J, \vec{H} , and $\Psi(\vec{r})$ denote the Landé factor of the localized spins and bound carriers, the spd-df exchange integral, the external magnetic field, and a trial wave function to be determined by a variational method, respectively. If the polaron contribution to F_p becomes comparable or larger than the carrier binding energy in the absence of exchange coupling, the probability of magnetization distribution $P_S[\vec{M}(\vec{r})]$ has to be taken beyond the Gaussian approximation [36, 37].

As we develop here the BMP theory for antiferromagnets and altermagnets with axial symmetry along the crystal c-axis, the relevant material parameters t, such as magnetic susceptibility χ for the multidomain case, effective mass m^* , carrier Landé factor g^* and exchange integral J assume a diagonal tensor form, t_a , t_a , t_c (where $t = \chi, m^*, g^*, J$). It is also convenient to introduce a tensor of bound carrier spin-splitting, in the absence of the

BMP contribution, generated by macroscopic magnetization $M_0^{(i)}(T, H_i)$ and the external magnetic field H_i applied along the direction i = a or c,

$$\Delta_0^{(i)} = J_i M_0^{(i)}(T, H_i) / g\mu_{\rm B} + g_i^* \mu_{\rm B} H_i, \tag{5}$$

where in antiferromagnets at $T < T_{\rm N}$, typically, $M_0^{(i)}(T,H_i) = \chi_i(T)H_i$ up to reaching a saturation value $M_{\rm SAT}$. We also introduce the tensor of the BMP energy,

$$\varepsilon_p^{(i)} = \frac{J_i^2 \chi_i}{4g^2 \mu_{\rm B}^2} \int d\vec{r} |\Psi(\vec{r})|^4, \tag{6}$$

where $\chi_i = \partial M_i / \partial H_i$. Making use of the identity,

$$\cosh x = \frac{d}{d\lambda_0} \frac{1}{4\pi\lambda_0} \int d^3 \lambda \delta(\lambda - \lambda_0) \exp\left(\vec{\lambda} \cdot \vec{x}\right) |_{\lambda_0 = 1}, (7)$$

we obtain

$$F_p = -k_{\rm B}T \ln \left(\frac{1}{2\pi} \left[\Theta'(1) - \Theta(1)\right]\right),\tag{8}$$

where, introducing $b(\vec{r}) = J|\Psi(\vec{r})|^2/2g\mu_{\rm B}$,

$$\Theta(\lambda_0) = \int_{\lambda = \lambda_0} d^2 \lambda \exp\left[\frac{1}{k_{\rm B}T} \int d^3 r (F_S(0) - F_S(\vec{\lambda}b(\vec{r})))\right].(9)$$

Here, $F_S(\vec{H})$ is the localized spins' free energy in the magnetic field \vec{H} , which can be obtained by inverting the experimental dependence $\vec{M}_0(T, \vec{H})$ into $\vec{h}(\vec{M})$ according to [36],

$$F(\vec{M}_0) = \int_0^{\vec{M}_0} d\vec{M} \vec{h}(\vec{M}) - \vec{H} \vec{M}_0, \tag{10}$$

where $\vec{M}_0 = \vec{M}_0(\vec{H})$. Now, in the linear approximation $-\nabla_{\vec{H}} F_S(\vec{H}) = \hat{\chi} \vec{H}$, we arrive at,

$$F_{p}(\vec{H}=0) = -\frac{1}{2}\varepsilon_{p}^{(a)} - k_{\rm B}T \ln \left\{ 2 \exp \left(\frac{\delta \varepsilon_{p}}{2k_{\rm B}T} \right) + \frac{\varepsilon_{p}^{(a)}}{k_{\rm B}T} \sqrt{\frac{2\pi k_{\rm B}T}{\delta \varepsilon_{p}}} \operatorname{erfi} \left(\sqrt{\frac{\delta \varepsilon_{p}}{2k_{\rm B}T}} \right) \right\}, \quad (11)$$

where $\delta \varepsilon_p = \varepsilon_p^c - \varepsilon_p^a$. By performing analogous calculations, it can be shown that

$$F_{p}(\vec{H}||\vec{c}) = -\frac{1}{2}\varepsilon_{p}^{a} + \frac{\Delta_{0}^{c}^{2}}{8\delta\varepsilon_{p}}$$
$$-k_{B}T \ln\{[1 + \exp(\Delta_{0}^{c}/k_{B}T)] \exp\left[\frac{(\Delta_{0}^{c} - 2\delta\varepsilon_{p})^{2}}{8k_{B}T\delta\varepsilon_{p}}\right]$$
$$-\frac{\varepsilon_{p}^{a}}{2k_{B}T}\sqrt{\frac{2\pi k_{B}T}{\delta\varepsilon_{p}}} \left[\operatorname{erfi}(\xi_{-}) - \operatorname{erfi}(\xi_{+})\right]\}, \tag{12}$$

where $\xi_{\pm} = (\Delta_0^c \pm 2\delta\varepsilon_p)/2\sqrt{2k_{\rm B}T\delta\varepsilon_p}$ and $F_p(\vec{H} \perp \vec{c})$ is given by formula (8), where

$$\Theta(\lambda_0) = 2\pi \lambda_0^2 \exp\left(\frac{\varepsilon_p^a}{2k_{\rm B}T}\lambda_0^2\right)$$

$$\times \int_{-1}^1 dt \, \exp\left(\frac{\delta \varepsilon_p \lambda_0^2 t^2}{2k_{\rm B}T}\right) I_0\left(\frac{\lambda_0 \Delta_0^a \sqrt{1-t^2}}{2k_{\rm B}T}\right) (13)$$

where I_0 is the 0th order modified Bessel function. We have checked that for $\delta \varepsilon_p = 0$, we recover the previously found form [20],

$$F_{p} = -\frac{\varepsilon_{p}}{2} - k_{\rm B}T \ln \left[2 \cosh \left(\frac{\Delta_{0}}{2k_{\rm B}T} \right) + \frac{4\varepsilon_{p}}{\Delta_{0}} \sinh \left(\frac{\Delta_{0}}{2k_{\rm B}T} \right) \right]$$
(14)

As trial functions we take $\Psi(\vec{r}) = (\pi c^* a^{*2})^{-1/2} \exp(-\sqrt{(\rho/a^*)^2 + (z/c^*)^2})$, where a^* and c^* are the bound carrier radii in the c-plane and along the c-axis, respectively. We also assume an anisotropic effective mass tensor and a spherically symmetrical impurity potential, as we assume the anisotropy of the dielectric constant is relatively small based on statistical data for various hexagonal crystals [38]. In order to obtain the localization radii, the total BMP free energy, $E_{\rm imp} + F_p$ is minimized with respect to a^* and c^* .

It should be noted that the results above assume a linear dependence $\vec{M}(\vec{H})$, which is valid provided that $|\vec{M}| < M_{\rm SAT} = Sg\mu_B N_S$ when calculating Θ from Eq. (9). This inequality may, however, be violated – but only for Bohr radii a^*, c^* satisfying

$$c^* a^{*2} \le \frac{\max(J_c \chi_c, J_a \chi_a)}{2\pi g \mu_0 \mu_B M_{\text{SAT}}}.$$
 (15)

If the susceptibilities χ_i are small enough (like for MnTe), the condition (15) is not satisfied for any a^*, c^* of realistic magnitudes; one can therefore perform calculations by neglecting the existence of a magnetization upper bound $M_{\text{SAT}} \to \infty$, and numerically find the correct localization radii. Otherwise, formulas for F_p need to be modified by, e.g., setting $\vec{M} = M_{\text{SAT}} \vec{H}/|\vec{H}|$ for $|\hat{\chi}\vec{H}| > M_{\text{SAT}}$. This approach will be used in numerical calculations for EuTe.

The determined free energy $F_p(T, H)$ provides directly the BMP contribution to the specific heat and magnetization [20, 21, 39] as well as to the activation energy of conductivity [40]. In view of anticipated experiments on spin-flip Raman scattering [22, 41] and optical absorption [42], we provide the expected probability distribution of bound carrier spin splitting,

$$P_p(\vec{\Delta}) = Z^{-1} 2 \cosh(\Delta/2k_{\rm B}T)$$

$$\times \exp\left[-\frac{(\Delta_c - \Delta_0^c)^2}{8k_{\rm B}T\varepsilon_p^c} - \frac{(\vec{\Delta}_a - \vec{\Delta}_0^a)^2}{8k_{\rm B}T\varepsilon_p^a}\right], \quad (16)$$

where Z is a normalization constant and $\Delta = (\Delta_c^2 + \vec{\Delta}_a^2)^{1/2}$. In the experimentally relevant case, $\Delta \gg k_{\rm B}T$

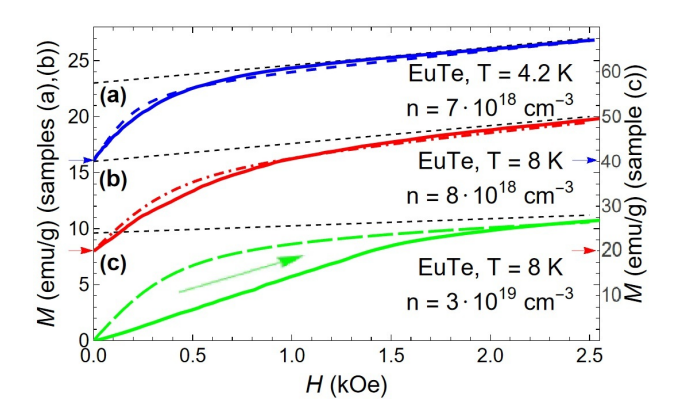


FIG. 1. Dependence of the magnetic moment per gram M on the magnetic field calculated from Eq. 17 (dashed curves) compared to experimental results (solid curves) at (a) 4.2 K [27] and (b),(c) 8 K [28]. The fitted BMP concentrations n are display in the legend. The straight dotted lines show a linear asymptotic behavior and provide the magnitude of magnetic susceptibility χ . An offset 16 and 8 emu/g was added to (a),(b) respectively for readability - two arrows next to the vertical axis indicate the positions of M=0 for those two plots.

and $\varepsilon_p^c \gg \varepsilon_p^a$ the most probable value of the spin splitting $\bar{\Delta} = \Delta_0^c + 2\varepsilon_p^c$. Under these conditions, $F_p = -\Delta_0^c/2 - \varepsilon_p^c/2$, as the formation of magnetic polaron lowers both the energy and entropy.

Comparison to experimental results for EuTe and MnTe. We first present results of numerical calculations for cubic antiferromagnetic EuTe without any long-range order in the Néel vector orientation, for which $\hat{\chi}$ and J are reduced to scalars; so that $a^* = c^*$ has been assumed in the family of trial functions. However, a rather large magnitude of magnetic susceptibility, resulting from a low value of $T_{\rm N}=9.6\,{\rm K}$, makes the magnetization generated by BMP attain locally the saturation value M_{SAT} , which has to be incorporated into the form of the functional $\mathcal{F}_S[M(\vec{r})]$, as already mentioned. A consensus has emerged that the conduction band in EuO and Eu monochalcogenides is built of Eu d orbitals for which the intra-atomic potential exchange $J_{5d4f}=215\,\mathrm{meV}$ [43]. This atomic value compares favorably with the observed and theoretical magnitudes of exchange band splitting in EuO J = 170 [44] and $230 \,\mathrm{meV}$ [45], respectively. We adopt, therefore, $J = 0.2 \,\mathrm{eV}$ together with $m^* = 0.3 m_e$, $\epsilon = 6.9, \ N_0 = 4/a^3 = 1.4 \times 10^{22} \, \mathrm{cm}^{-3}$ (like in [46]), $\chi = 1.61 \times 10^{-3} \, \mathrm{emu/gOe}$ (slope of M(H) for samples without BMPs [27, 28]), and $g^* = g = 2.0$, the latter expected for both Eu⁺² and Mn⁺² in the orbital singlet configuration. For these parameters, we determine magnetization according to,

$$M(H) = -n\partial F_p/\partial H + \chi H, \tag{17}$$

where n is the bound carrier concentration that, in general, may depend on temperature, and F_p is calculated for a^* resulting from minimization of F_p with respect to

 a^* .

Figure 1 presents a comparison of our theoretical results to experimental data for EuTe below Néel temperature [27, 28]. As cubic anisotropy is typically small, even allowing for a larger magnitude of magnetic susceptibility in the plane perpendicular to the local Néel vector, magnetization brought about by BMPs should show no hysteresis and vanish in the absence of a magnetic field. However, in H > 0, BMPs' magnetic moments align along the magnetic field, and the BMP contribution shows up. Importantly, this additional magnetization was observed neither for metallic samples [47] nor for a sample with an unmeasurably low electron concentration n_e at 300 K [28], which supports its interpretation in terms of BMPs. The agreement between theory and experiment is quite good for samples with donor densities below 10^{19} cm^{-3} [plots (a),(b)]. For $n_e = 4 \times 10^{18} \text{ cm}^{-3}$ [28], we find $n = 8 \times 10^{18} \text{ cm}^{-3}$, as in this strongly localized case room temperature electron concentration is presumably smaller than the bound carrier density at helium temperatures. In contrast, the agreement is poor for the sample with the highest value of $n_e = 6 \times 10^{19} \,\mathrm{cm}^{-3}$ [28] [plot (c)], probably due to interactions between BMPs. The obtained effective Bohr radius $a^* = 0.71 \,\mathrm{nm}$ leads then to $n_e^{1/3}a^* = 0.28$, which somewhat surpasses the Mott critical value 0.26 marking the delocalization transition. Accordingly, the low-temperature BMP concentration determined from magnetization data in Fig. 1 is smaller, $n = 3 \times 10^{19} \,\mathrm{cm}^{-3}$, as only bound carriers with energies below the mobility edge form BMPs.

We now turn to the numerical analysis of BMP magnetic properties in bulk hexagonal p-type MnTe. We assume $q^* = q = 2.0$ and take the values of dielectric constant, lattice parameters, magnetic susceptibility, and effective mass tensor from Refs. 30–32, and 48. The J tensor has been obtained by a method applied previously for (Cd,Mn)Te and (Hg,Mn)Te [49] with the implementation of the density functional theory described elsewhere [50]. In agreement with previous results [51], we find the valence band maximum at the A point of the Brillouin zone and determine the magnitude of the band splitting for the ferromagnetic arrangement of Mn spins. As shown in Fig. 2, exchange splitting of the topmost valence band at the A point corresponds to $J_a = J_c = -0.5 \,\text{eV}$. This time, since the magnetic susceptibilities along and perpendicularly to the c-axis are significantly smaller than χ_{EuTe} , there is no need to allow for a finite value of M_{SAT} .

Under thermal equilibrium and in H=0, BMP average magnetization vanishes due to symmetry, while for $H\to\infty$ BMP moments are aligned along the magnetic field. However, uniaxial anisotropy of magnetic susceptibility at $T< T_{\rm N}$ can result in a hysteretic behavior of BMP magnetization when cycling the external magnetic field. According to the Stoner-Wolfarth model, the coercivity field $H_c=2K/m$, where the anisotropy energy K is given by a difference between the BMP free energy for the BMP magnetic moment m aligned along the hard

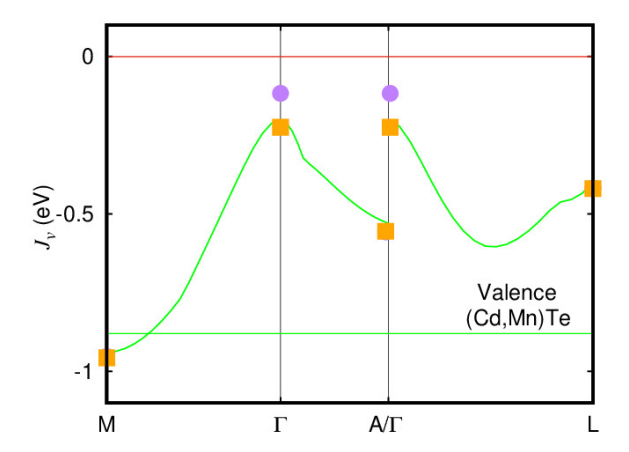


FIG. 2. Computed exchange energy J_v for the valence band of MnTe in the non-relativistic case (green lines) and in the relativistic case with saturated magnetization along the a-axis (purple dots) and along the c-axis (orange triangles). The horizontal line is the experimental value of J_v at the Γ point of the valence band in (Cd,Mn)Te (see, Ref. 49).

and easy axis,

$$K = \lim_{H \to \infty} [F_p(\vec{H} \perp \vec{c}) - F_p(\vec{H} || \vec{c})].$$

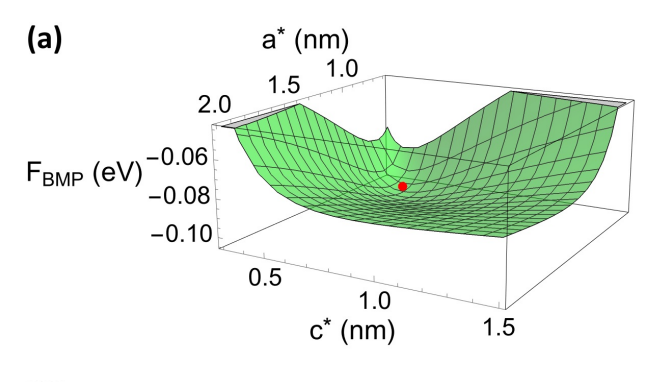
The BMP magnetic moment is determined from Eq. (12) as.

$$m = -\partial F_p/\partial H|_{H\to\infty} = \frac{1}{2}|g_c^*\mu_{\rm B} + J_c\chi_c/g\mu_{\rm B}|, \quad (18)$$

so that, within our model, the remanent magnetization for the magnetic field cycled along the c axis is expected to be determined by $M_{\rm REM}=nm$.

Figure 3 presents the numerical implementation of the BMP theory for bulk MnTe at experimental temperature $T=250\,\mathrm{K}$ [32] – the dependence of BMP free energy in H=0 on the effective localization radii a^*,c^* and the dependence of F_p minimized with respect to a^*,c^* on \vec{H} . For instance, $a^*=0.89\,\mathrm{nm},\,c^*=0.54\,\mathrm{nm}$ for H=0; these values depend rather weakly on H in the considered range, but it should be noted that they are quite sensitive to the values of m^* and ϵ . These values and the Mott condition $(na^{*2}c^*)^{1/3}=0.26$ imply that the delocalization transition occurs at $n=4\times10^{19}\,\mathrm{cm}^{-3}$.

Carrier localization at low temperatures and the presence of the anomalous Hall effect make the determination of the bound carrier concentration difficult. The experimental value $M_{\rm REM} \sim 5 \times 10^{-5} \, \mu_{\rm B}/{\rm Mn}$ [32] implies, within our model, $n \simeq 10^{16} - 10^{17} \, {\rm cm}^{-3}$ at 250 K. This evaluation constitutes an upper limit, as one expects that magnetization brought about by weak ferromagnetism specific to MnTe will align with the BMP magnetic moment. Obviously, studies of remanent magnetization as a function of bound carrier concentration would allow to



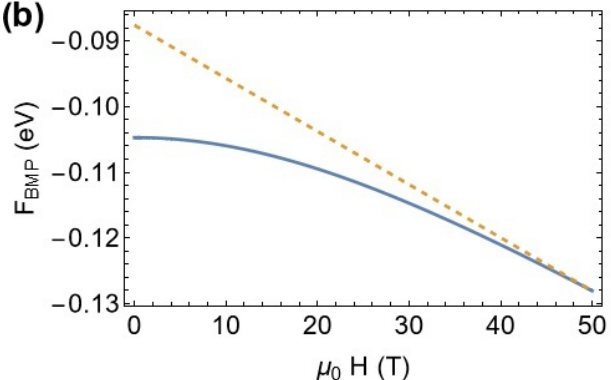


FIG. 3. (a) dependence of BMP free energy F_p on the effective Bohr radii along the c-axis (c^*) and in the c-plane (a^*) . The red point depicts a minimum found by the variational procedure. (b) dependence of the BMP free energy (minimized with respect to radii a^* and c^*) on the magnetic field H applied along the c-axis. The straight line is a linear asymptote corresponding to BMP's magnetic moment parallel to the magnetic field. Temperature $T=250\,\mathrm{K}$ for both plots.

verify the role of BMPs. Within our model, we also obtain $K=0.9\,\mathrm{meV}$ and $H_c=21\,\mathrm{kOe}$ at that temperature, which appears to compare favorably with the experimental value $H_c=25\pm5\,\mathrm{kOe}$ [32, 33] but leads to rather low superparamagnetic blocking temperature T_B . Neglecting coupling between BMPs, $K>0.4\,\mathrm{eV}$ would lead to $T_\mathrm{B}>250\,\mathrm{K}$. Actually, strong anisotropy of weak ferromagnetism magnetization [50] and the exchange bias by surrounding antiferromagnetic lattice [16, 52] can enhance the magnitude of K considerably. In particular, the exchange coupling causes a distortion of the antiferromagnetic spin lattice in the range of the order of $(|J|/K_c)^{1/6}$ lattice sites [16], where J, K_c are exchange

integrals between neighboring Mn ions and crystalline anisotropy, respectively. For $|J|/K_c \sim 2500$, as in the spin canting modelling [32], we find that the distortion extends over 3-4 lattice sites, i.e., involves $\sim 600-700$ Mn ions, to be compared to around 40 spins in the BMP volume $4\pi a^{*2}c^*/3$. The resulting coupling between BMPs will enhance the K value even more.

Conclusions and outlook. We have introduced a new ingredient into the physics of altermagnetic semiconductors, namely the bound magnetic polarons. In the case of single-domain microstructures, BMP magnetization will compete with intrinsic weak ferromagnetism [50] allowed for some altermagnets in the presence of a spin-orbit interaction [53]. In the multidomain situation, non-zero magnetization resulting from weak ferromagnetism cancels out, leaving the BMP contribution to dominate, most probably the case of MnTe samples discussed here, taking into account the results of nanoscale magnetization imaging of MnTe [54]. However, the presence of local weak magnetization will lead to an additional shift or broadening of the BMP spin-resonance line. Hence, spin-flip Raman scattering and related techniques could constitute a valuable tool for probing magnetization distribution and dynamics of altermagnetic semiconductors at the nanoscale. We also note that the presence of large bound carrier spin-splitting in Raman scattering, but significantly smaller magnetization than predicted here, will imply that we deal with a compensated magnet [55] or an altermagnet allowing for zero-field exchange splitting at the relevant band extremum.

ACKNOWLEDGEMENTS

This research was supported by the "MagTop" project (FENG.02.01-IP.05-0028/23) carried out within the "International Research Agendas" programme of the Foundation for Polish Science co-financed by the European Union under the European Funds for Smart Economy 2021-2027 (FENG). We further acknowledge access to the computing facilities of the Interdisciplinary Center of Modeling at the University of Warsaw, Grant g91-1418, g91-1419, g96-1808 and g96-1809 for the availability of high-performance computing resources and support.

DATA AVAILABILITY

The data that support the findings of this article are openly available [56].

L. Šmejkal, J. Sinova, and T. Jungwirth, Emerging research landscape of altermagnetism, Phys. Rev. X 12, 040501 (2022).

^[2] L. Bai, W. Feng, S. Liu, L. Šmejkal, Y. Mokrousov, and Y. Yao, Altermagnetism: Exploring new frontiers in mag-

netism and spintronics, Adv. Funct. Mater. 34, 2409327 (2024).

^[3] T. Dietl and H. Ohno, Dilute ferromagnetic semiconductors: Physics and spintronic structures, Rev. Mod. Phys. 86, 187 (2014).

- [4] T. Jungwirth, J. Wunderlich, V. Novák, K. Olejník, B. L. Gallagher, R. P. Campion, K. W. Edmonds, A. W. Rushforth, A. J. Ferguson, and P. Němec, Spin-dependent phenomena and device concepts explored in (Ga,Mn)As, Rev. Mod. Phys. 86, 855 (2014).
- [5] E. L. Nagev, Magnetic polarons (ferrons) of complicated structure, JETP Letters 74, 431 (2001).
- [6] A. Kłosiński, D. V. Efremov, J. van den Brink, and K. Wohlfeld, Photoemission spectrum of: Spin polaron physics in an antiferromagnet with anisotropies, Phys. Rev. B 101, 035115 (2020).
- [7] P. Wrzosek, A. Kłosiński, Y. Wang, M. Berciu, C. E. Agrapidis, and K. Wohlfeld, The fate of the spin polaron in the 1D antiferromagnets, SciPost Phys. 17, 018 (2024).
- [8] A. Bohrdt, F. Grusdt, and M. Knap, Dynamical formation of a magnetic polaron in a two-dimensional quantum antiferromagnet, New J. Phys. 22, 123023 (2020).
- [9] K. K. Nielsen, M. A. Bastarrachea-Magnani, T. Pohl, and G. M. Bruun, Spatial structure of magnetic polarons in strongly interacting antiferromagnets, Phys. Rev. B 104, 155136 (2021).
- [10] J. H. Nyhegn, G. M. Bruun, and K. K. Nielsen, Wave function and spatial structure of polarons in an antiferromagnetic bilayer, Physical Review B 108, 075141 (2023).
- [11] C. R. W. Steward, R. M. Fernandes, and J. Schmalian, Dynamic paramagnon-polarons in altermagnets, Phys. Rev. B 108, 144418 (2023).
- [12] F. C. Zhang and T. M. Rice, Effective Hamiltonian for the superconducting Cu oxides, Phys. Rev. B 37, 3759 (1988).
- [13] A. Mauger and D. L. Mills, Bound magnetic polarons in antiferromagnetic semiconductors, Phys. Rev. Lett. 53, 1594 (1984).
- [14] L. Liu and J. T. C. Liu, Theory of the bound magnetic polaron in antiferromagnetic semiconductors, Phys. Rev. B 33, 1797 (1986).
- [15] L. Liu, Theory of magnetic polarons in antiferromagnetic semiconductors, Phys. Rev. B 37, 5387 (1988).
- [16] J. Castro, I. González, and D. Baldomir, Stabilization of magnetic polarons in antiferromagnetic semiconductors by extended spin distortions, The European Physical Journal B 39, 447 (2004).
- [17] S. L. Ogarkov, M. Y. Kagan, A. O. Sboychakov, A. L. Rakhmanov, and K. I. Kugel, Formation of long-range spin distortions by a bound magnetic polaron, Phys. Rev. B 74, 014436 (2006).
- [18] M. Y. Kagan, S. L. Ogarkov, K. I. Kugel, A. O. Sboy-chakov, and A. L. Rakhmanov, Bound magnetic polarons with extended spin distortions on frustrated lattices, J. Phys.: Condensed Matter 20, 425214 (2008).
- [19] A. B. Henriques, S. C. P. van Kooten, E. Abramof, P. H. O. Rappl, and G. D. Galgano, Bound photoinduced giant spin polaron in EuTe, J. Appl. Phys. 131, 043903 (2022), see also references cited therein.
- [20] T. Dietl and J. Spalek, Effect of fluctuations of magnetization on the bound magnetic polaron: Comparison with experiment, Phys. Rev. Lett. 48, 355 (1982).
- [21] T. Dietl and J. Spałek, Effect of thermodynamic fluctuations of magnetization on the bound magnetic polaron in dilute magnetic semiconductors, Phys. Rev. B 28, 1548 (1983).
- [22] D. Heiman, P. A. Wolff, and J. Warnock, Spin-flip Raman scattering, bound magnetic polaron, and fluctuations in (Cd,Mn)Se, Phys. Rev. B 27, 4848 (1983).

- [23] T. Dietl, Spin dynamics of a confined electron interacting with magnetic or nuclear spins: A semiclassical approach, Phys. Rev. B 91, 125204 (2015).
- [24] T. Dietl, (Diluted) magnetic semiconductor, in *Hand-book on Semiconductors*, Vol. 3B, edited by S. Mahajan (North-Holland, Amsterdam 1994, 1994) p. 91251.
- [25] M. Gaudin, Diagonalisation d'une classe d'hamiltoniens de spin, J. Phys. France 37, 1087 (1976).
- [26] E. De Nadai, N. Maestracci, and A. Faribault, Integrability and dark states of the XX spin-1 central spin model in a transverse field, Phys. Rev. B 110, 205427 (2024).
- [27] N. F. Oliveira, S. Foner, Y. Shapira, and T. B. Reed, EuTe. I. magnetic behavior of insulating and conducting single crystals, Phys. Rev. B 5, 2634 (1972).
- [28] J. Vitins and P. Wachter, Doped EuTe: A mixed magnetic system, Phys. Rev. B 12, 3829 (1975).
- [29] T. Komatsubara, M. Murakami, and E. Hirahara, Magnetic properties of manganese telluride single crystals, J. Phys. Soc. Jpn. 18, 356 (1963).
- [30] G. Zanmarchi and C. Haas, Magnon drag, Philips Research Reports 23, 389 (1968).
- [31] W. Szuszkiewicz, B. Hennion, B. Witkowska, E. Lusakowska, and A. Mycielski, Neutron scattering study of structural and magnetic properties of hexagonal MnTe, phys. stat. sol. (c) 2, 1141 (2005).
- [32] K. P. Kluczyk, K. Gas, M. J. Grzybowski, P. Skupiński, M. A. Borysiewicz, T. Fas, J. Suffczyński, J. Z. Domagala, K. Grasza, A. Mycielski, M. Baj, K. H. Ahn, K. Výborný, M. Sawicki, and M. Gryglas-Borysiewicz, Coexistence of anomalous Hall effect and weak magnetization in a nominally collinear antiferromagnet MnTe, Phys. Rev. B 110, 155201 (2024).
- [33] R. D. Gonzalez Betancourt, J. Zubáč, R. Gonzalez-Hernandez, K. Geishendorf, Z. Šobáň, G. Springholz, K. Olejník, L. Šmejkal, J. Sinova, T. Jungwirth, S. T. B. Goennenwein, A. Thomas, H. Reichlová, J. Železný, and D. Kriegner, Spontaneous anomalous Hall effect arising from an unconventional compensated magnetic phase in a semiconductor, Phys. Rev. Lett. 130, 036702 (2023).
- [34] I. I. Mazin and K. D. Belashchenko, Origin of the gossamer ferromagnetism in mnte, Phys. Rev. B 110, 214436 (2024).
- [35] C. Autieri, R. M. Sattigeri, G. Cuono, and A. Fakhredine, Staggered Dzyaloshinskii-Moriya interaction inducing weak ferromagnetism in centrosymmetric altermagnets and weak ferrimagnetism in noncentrosymmetric altermagnets, Phys. Rev. B 111, 054442 (2025).
- [36] L. Świerkowski and T. Dietl, Stability of self-trapped magnetic polarons, Acta Phys. Polon. A 73, 431 (1988).
- [37] C. Benoit à la Guillaume, Free magnetic polarons in three, quasi-two, and quasi-one dimensions, phys. stat. sol. (b) 175, 369 (1993).
- [38] Y. Lou and A. M. Ganose, Discovery of highly anisotropic dielectric crystals with equivariant graph neural networks, Faraday Discuss. **256**, 255 (2025).
- [39] T. Wojtowicz, S. Koleśnik, I. Miotkowski, and J. K. Furdyna, Magnetization of bound magnetic polarons: Direct determination via photomemory effect, Phys. Rev. Lett. 70, 2317 (1993).
- [40] J. Jaroszyński and T. Dietl, Exchange splitting of acceptor states in semimagnetic-semiconductors: Magnetoresistance studies of $\mathrm{Cd}_{1-x}\mathrm{Mn}_x\mathrm{Te}$, Solid State Commun. **55**, 491 (1985).

- [41] M. Nawrocki, R. Planel, G. Fishman, and R. Galazka, Exchange-induced spin-flip Raman scattering in a semimagnetic semiconductor, Phys. Rev. Lett. 46, 735 (1981).
- [42] M. Dobrowolska, A. Witowski, J. K. Furdyna, T. Ichiguchi, H. D. Drew, and P. A. Wolff, Far-infrared observation of the electric-dipole spin resonance of donor electrons in $Cd_{1-x}Mn_xSe$, Phys. Rev. B **29**, 6652 (1984).
- [43] H. N. Russell, W. Albertson, and D. N. Davis, The spark spectrum of Europium, Eu II, Phys. Rev. **60**, 641 (1941).
- [44] P. G. Steeneken, L. H. Tjeng, I. Elfimov, G. A. Sawatzky, G. Ghiringhelli, N. B. Brookes, and D.-J. Huang, Exchange splitting and charge carrier spin polarization in EuO, Phys. Rev. Lett. 88, 047201 (2002).
- [45] W.-Y. Tong, H.-C. Ding, Y.-C. Gao, S.-J. Gong, X. Wan, and C.-G. Duan, Spin-dependent optical response of multiferroic euo: First-principles DFT calculations, Phys. Rev. B 89, 064404 (2014).
- [46] X. Gratens, Y. Ou, J. S. Moodera, P. H. O. Rappl, and A. B. Henriques, Hypergiant spin polarons photogenerated in ferromagnetic europium chalcogenides, Appl. Phys. Lett. 116, 152402 (2020).
- [47] Y. Shapira, S. Foner, N. F. Oliveira, and T. B. Reed, EuTe. II. Resistivity and Hall Effect, Phys. Rev. B 5, 2647 (1972).
- [48] J. Oleszkiewicz, A. Kisiel, and S. A. Ignatowicz, Optical properties and dielectric function of manganese telluride thin films, Thin Solid Films 157, 1 (1988).
- [49] C. Autieri, C. Śliwa, R. Islam, G. Cuono, and T. Dietl, Momentum-resolved spin splitting in mn-doped trivial

- CdTe and topological HgTe semiconductors, Phys. Rev. B 103, 115209 (2021).
- [50] C. C. Ye, K. Tenzin, J. Sławińska, and C. Autieri, Dominant orbital magnetization in the prototypical altermagnet MnTe (2025), arXiv:2505.08675.
- [51] P. E. Faria Junior, K. A. de Mare, K. Zollner, K.-h. Ahn, S. I. Erlingsson, M. van Schilfgaarde, and K. Výborný, Sensitivity of the MnTe valence band to the orientation of magnetic moments, Phys. Rev. B 107, L100417 (2023).
- [52] V. Skurmyev, S. Stoyanov, Y. Zhang, G. Hadjipanayis, D. Givors, and J. Nogués, Beating the superparamagnetic limit with exchange bias, Nature 423, 850 (2003).
- [53] S.-W. Cheong and F.-T. Huang, Altermagnetism classification, npj Quantum Materials **10**, 38 (2025).
- [54] O. J. Amin, A. Dal Din, E. Golias, Y. Niu, A. Za-kharov, S. C. Fromage, C. J. B. Fields, S. L. Heywood, R. B. Cousins, F. Maccherozzi, J. Krempaský, J. H. Dil, D. Kriegner, B. Kiraly, R. P. Campion, A. W. Rushforth, K. W. Edmonds, S. S. Dhesi, L. Šmejkal, T. Jungwirth, and P. Wadley, Nanoscale imaging and control of altermagnetism in MnTe, Nature 636, 348 (2024).
- [55] J. Finley and L. Liu, Spintronics with compensated ferrimagnets, Appl. Phys. Lett. 116, 110501 (2020).
- [56] Data presented in the figures and text are available at https://doi.org/10.5281/zenodo.15717079.